Scaling of heat transfer augmentation due to mechanical distortions in hypervelocity boundary layers

W. Flaherty and J. M. Austin

Citation: Physics of Fluids (1994-present) **25**, 106106 (2013); doi: 10.1063/1.4826476
View online: http://dx.doi.org/10.1063/1.4826476
View Table of Contents: http://scitation.aip.org/content/aip/journal/pof2/25/10?ver=pdfcov
Published by the AIP Publishing

PHYSICS OF FLUIDS **25**, 106106 (2013)

Scaling of heat transfer augmentation due to mechanical distortions in hypervelocity boundary layers

W. Flaherty and J. M. Austin
Department of Aerospace Engineering, University of Illinois, Urbana, Illinois 61801, USA

(Received 22 March 2013; accepted 2 October 2013; published online 30 October 2013)

We examine the response of hypervelocity boundary layers to global mechanical distortions due to concave surface curvature. Surface heat transfer and visual boundary layer thickness data are obtained for a suite of models with different concave surface geometries. Results are compared to predictions using existing approximate methods. Near the leading edge, good agreement is observed, but at larger pressure gradients, predictions diverge significantly from the experimental data. Up to a factor of five underprediction is reported in regions with greatest distortion. Curve fits to the experimental data are compared with surface equations. We demonstrate that reasonable estimates of the laminar heat flux augmentation may be obtained as a function of the local turning angle for all model geometries, even at the conditions of greatest distortion. This scaling may be explained by the application of Lees similarity. As a means of introducing additional local distortions, vortex generators are used to impose streamwise structures into the boundary layer. The response of the large scale vortices to an adverse pressure gradient is investigated. Surface streak evolution is visualized over the different surface geometries using fast response pressure sensitive paint. For a flat plate baseline case, heat transfer augmentation at similar levels to turbulent flow is measured. For the concave geometries, increases in heat transfer by factors up to 2.6 are measured over the laminar values. The scaling of heat transfer with turning angle that is identified for the laminar boundary layer response is found to be robust even in the presence of the imposed vortex structures. © *2013 AIP Publishing LLC*. [http://dx.doi.org/10.1063/1.4826476]

I. INTRODUCTION

Concave surface curvature can introduce significant distortion to compressible boundary layer flows due to multiple, potentially coupled, effects including an adverse pressure gradient, bulk flow compression, and possible centrifugal instabilities, see, for example, White,[1] Saric,[2] and Smits and Dussauge.[3] Solution strategies for the compressible boundary layer equations in the presence of a pressure gradient have been investigated by numerous researchers, and approximate methods have been developed that can provide insight into the dominant mechanisms. Only a few of these methods treat heat transfer effects.

One such approximate method for boundary layer calculations was developed by Cohen and Reshotko.[4] Stewartson's transformation was applied to the compressible boundary layer equations and unity Prandtl number; linear viscosity-temperature relationship and an isothermal surface were assumed. Thwaites[5] correlation was used to develop an approximate solution method.[6] In the case of a favorable pressure gradient, agreement was within 2% of predictions based on a perturbation method,[7] however for an adverse pressure gradient with an insulated wall, significant departure from perturbation theory was observed for predictions of skin friction and heat transfer. As noted by the authors, this departure appears consistent with the limitations of small-pressure gradient perturbation theory applied to a highly distorted flow, where their more general formation may be more reliable. No comparison with experimental data was reported.

The effects of self-induced pressure gradients due to viscous interaction for compressible, flat-plate boundary layers were examined by Li and Nagamatsu.[8] They arrived at their approach after

determining that the compressible pressure gradient parameter can be related to the incompressible form, assuming the flow is hypersonic (implying a small change in fluid velocity across the shock) and isentropic. This method was extended to include surface curvature by Bertram and Feller.[9] Reasonable agreement was obtained between computed results and experimental heat flux data for a favorable pressure gradient over a blunted flat plate. The Bertram and Feller method was modified by Crawford to accommodate a more general pressure profile.[10] Theoretical results were compared with experimental data for concave and convex shapes with a blunt leading edge. Good agreement was observed between theory and experiment, though the theory slightly over predicted heat flux in most cases. Though the available data set contained regions with strong adverse pressure gradients, predictions were only generated for favorable pressure gradient data.

In a study of heat transfer over blunted bodies with favorable pressure gradients, Lees identified that at hypersonic flight conditions the gas density near the surface is much higher than outside the boundary layer, and as a consequence the velocity and enthalpy profiles near the surface are much less sensitive to the pressure gradient than to the local pressure, leading to "local similarity" (Sec. III B 2).[11] Combining the local flat plate similarity theory of Lees[11] with the Newton-Busemann pressure approximation, Cheng[12] developed a theoretical model to predict boundary layer quantities on blunted flat plates at an angle of attack in hypersonic flow. This method was extended to curved surfaces by Stollery.[13] He found that the use of the Newton-Busemann pressure law caused large scale, non-physical oscillations, but these could be mitigated by substitution of the tangent-wedge pressure approximation. With the modified Cheng method, Stollery obtained good agreement between predictions and pressure measurements over a cubic concave ramp in a hypersonic gun tunnel. This method was again tested by Mohammadian[14] and compared with schlieren, surface pressure, and heat transfer data for a Mach 12.25 flow over a cubic ramp with cold wall. Near the leading edge, the modified Cheng method predictions agreed closely with heat transfer measurements, but by 4 in. downstream of the leading edge, in the region of larger turning angles (18°), the two diverged rapidly, with the theoretical model far over-predicting the experimental heat flux. In the presence of the strong adverse pressure gradient, Mohammadian proposed that the assumption of local flat plate similarity may fail and strong normal pressure gradients may exist.

The discrepancies in the predictions of heat transfer using approximate methods for boundary layers subjected to strong distortions due to adverse pressure gradients, and the sparsity of experimental data in these same flows, motivated the present study. We focus on hypervelocity flows where thermochemical processes may have a significant impact on boundary layer structure and stability, as previously demonstrated predominantly for flat plate boundary layers. For example, thermochemical equilibrium and nonequilibrium have been shown to affect boundary layer stability through modifications both to the mean flow and to the frequency and amplitude of growth rates.[15–17] Numerical predictions of surface heat flux at hypervelocity conditions are challenged by the accuracy with which gas and surface reaction rates are known, see, for example, Park[18] and Miller *et al.*[19]

Destabilization of a compressible boundary layer over a concave surface has also been demonstrated to augment the heat flux and skin friction significantly in turbulent boundary layer flows. Experiments by Donovan[20] in a Mach 2.9 turbulent flow showed the absolute wall shear stress increased by about 125% and the skin friction by about 77% over a concave wall. When compared to a previous study[21] of a flat plate boundary layer with the same pressure gradient imposed, the turbulence levels and skin friction were amplified by an additional 60%–70% due to the curvature. Experimental measurements indicated that the observed augmentation was not only due to the streamline curvature, adverse pressure gradients, and bulk compression, but these effects were coupled with strong amplification of the turbulent stresses. Fernando and Smits[22] investigated a flat plate with an imposed pressure gradient equal to that over a curved ramp. Significant differences in the velocity profiles and Reynolds stresses were measured, and an increase in the wall friction of 17% for the curved surface was reported. Ekoto *et al.*[23] studied the response of a turbulent boundary layer in a Mach 2.86 flow to favorable and combined pressure gradients caused by surface curvature. Local mechanical distortions in the form of two types of patterned roughness on the wall were also introduced and quantitative characterization of the interaction between turbulent flow structures and associated production mechanisms were carried out for the different combinations of local and global distortions.

Discrete roughness elements or protuberances can introduce local mechanical distortion and vortices to the boundary layer. Multiple different roughness geometries were investigated by Whitehead.[24] Oil flow patterns showed upstream flow separation and multiple vortex filaments which were wrapped around the protuberance and swept downstream to form horseshoe vortex structures. The effects of a discrete protuberance have been investigated by Sedney,[25] among others. For high speed flow, transition to turbulence was not necessarily observed even when the roughness height was comparable to the boundary layer thickness. In these cases where laminar flow was maintained, the flowfield was still significantly distorted by the vortices generated by the roughness element. A single protuberance in a hypersonic flow was examined experimentally by Danehy *et al.*[26] and numerically by Chang and Choudhari.[27] The simulations showed that vorticity is formed in the recirculation region in front of the roughness element, and the resulting vortex filament propagates downstream as a horseshoe vortex after wrapping around the sides of the protuberance. Almost no vortex shedding over the element was observed, and the spanwise influence was determined to extend almost five roughness diameters away from the element.

In the present work, we investigate the response of hypervelocity boundary layers to a region of concave surface curvature. A suite of models with different surface geometries and final turning angles are selected. We first examine the response of laminar boundary layers and carry out a comparative study of the heat flux augmentation. In addition, vortex generators are used to introduce streamwise structures into the boundary layer as a model problem to examine the interaction of global and local mechanical distortions. Diagnostics include surface heat transfer and visual boundary layer profile measurements, as well as pressure sensitive paint visualizations of streak patterns created by the imposed vortices.

II. EXPERIMENTAL SETUP

A. Facility description and test conditions

Experiments were carried out in the Hypervelocity Expansion Tube (HET). The 9.14 m long facility consists of driver, driven, and accelerator sections all with a 150 mm inner diameter. In an expansion tube, gas acceleration to hypervelocity conditions is achieved in two stages using a shock wave and an unsteady expansion fan. The first two sections of the facility, the driver and driven, are initially separated by a 1.27 mm thick aluminum diaphragm. Upon rupture of the diaphragm, a shock propagates into the quiescent driven gas. The defining feature of an expansion tube is the third section, known as the accelerator. The accelerator is initially separated from the driven section by a plastic diaphragm which is 0.0127 mm thick. Rupture of the diaphragm by the incident shock generates a transmitted shock and reflected expansion fan. The shock-accelerated driven gas encounters the unsteady expansion fan and is accelerated to hypervelocity conditions. The test time begins with the arrival of the contact surface between the accelerator and the driven gas. Termination of the test time for the conditions of the current study occurs with the arrival of the expansion tail (for test time calculation procedures see Dufrene *et al.*[28]). The HET facility can access a range of Mach numbers from 3.0 to 7.5 and stagnation enthalpies from 4 to 9 MJ/kg.

TABLE I. Theoretical parameters for HET test conditions used in this study.

Condition	Air-4	Air-5
Mach number	5.12	7.45
Static temperature (K)	676	642
Static pressure (kPa)	8.13	0.77
Velocity (m/s)	2664	3779
Density (kg/m^3)	0.042	0.004
Test time (μs)	361	163
Unit Reynolds number (1/m)	3.42×10^6	0.5×10^6
Stagnation enthalpy (MJ/kg)	4.08	7.65

TABLE II. Model specifications. G is the Goertler number at the initiation of curvature.

Model	Radius (mm)	Turning angle (deg)	Curvature length (mm)	G
Flat plate	...	0	0	...
Curved10	908	10.5	165	6.4
Curved16	350	16	100	10.3
Curved25	330	25	140	10.6
Curved30	113	30	57	18.1
Cubic32	...	32	165	2

Two test conditions, denoted as Air-4 and Air-5, were selected for this study. The Air-4 test condition has a Reynolds number and test time which are on the high end of what is attainable in the tube. The Air-5 condition has a much lower Reynolds number and test time, but has a higher Mach number than the Air-4 condition. Theoretical free stream conditions calculated using unsteady, one-dimensional gas dynamics for both test conditions are given in Table I. For more information on the design, operation, and verification of the HET, refer to Dufrene *et al.*[28]

B. Experimental models

A suite of six interchangeable models were used for this study. Details of the model geometries are given in Table II, together with the nomenclature used in this paper. A sketch of the model with basic features highlighted is shown in Figure 1. Models were chosen to span a range of turning angles, therefore covering multiple imposed distortions of different strengths. The surface equations of these models were also varied (i.e., cubic or quadratic). The Curved16 model was designed to replicate the model used in Donovan *et al.*[20] Curved10, Curved16, Curved25, and Cubic32, denoted in this work as the "large" models have a 248 mm long and 65 mm wide footprint. These models used the same mounting system so that the surface geometry could be exchanged without introducing any variable leading edge effects. The sting mounting system incorporated a sharp leading edge followed by a 83 mm flat plate section, which allowed the boundary layer to develop before encountering any modification to the surface geometry. A thermocouple was placed in the flat plate region of each model, creating a common data point to ensure there was no unexpected variation in the test condition. As a baseline case, a flat plate model could also be mounted to replace the concave geometries.

The models also included a location to mount a row of diamond vortex generators 76 mm behind the leading edge of the model (right at the beginning of curvature) (Figure 2(a)). The strip of vortex generators consisted of 11 elements spaced evenly along the span of the model. One element was located along the centerline of the model. The vortex generators were based on the design of Berry *et al.*[29] These diamond roughness elements were scaled to two boundary layer thicknesses (boundary layer thickness at 76 mm from the leading edge was estimated to be around 1.27 mm), as shown in Figure 2(b). Some parameters of interest to roughness elements are listed in Table III.

Due to the decreased test time in the Air-5 test condition in the HET, it was not possible to establish steady flow over the larger models. Curved30 was designed as a shorter ("small") model

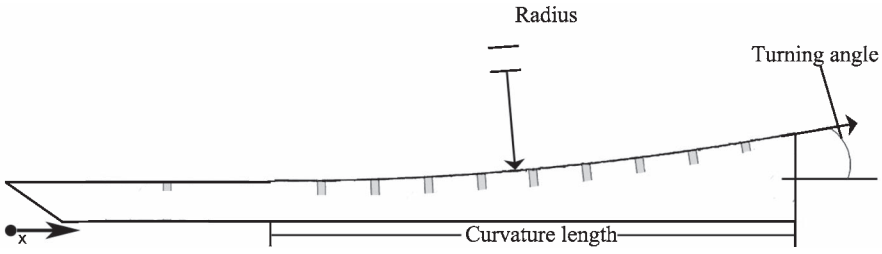

FIG. 1. Sketch highlighting major features of the curved ramp models.

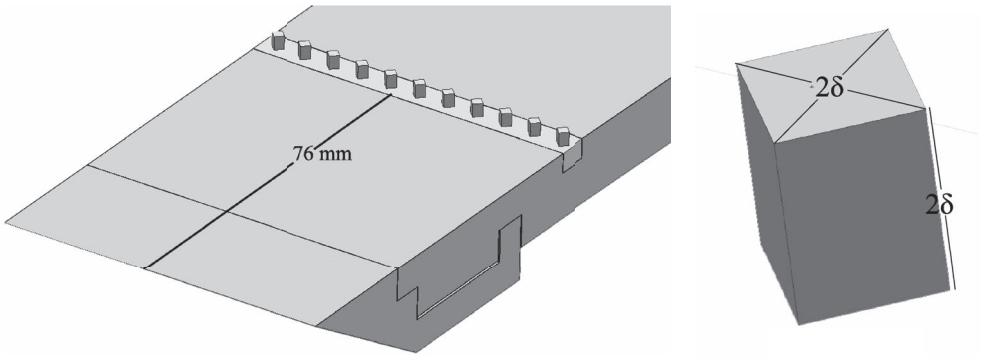

FIG. 2. (a) Model of the vortex generator strip mounted in the flat plate. (b) Model of a single vortex generator element.

such that data could be obtained for the Air-5 condition. A decreased radius of curvature was used for this model to achieve a measurable increase in heat transfer over the shorter distance. Unfortunately, the decreased radius of curvature for the Curved30 model also results in the formation of a shock nearer the boundary layer in the Air-4 condition, thus this model was only tested in Air-5. The Curved30 model has a footprint 129 mm long and 65 mm wide. It was designed with a shorter (25.4 mm) flat plate region behind the leading edge. A simplified sketch highlighting the basic features of the flow over the curved models is shown in Figure 3.

C. Diagnostics, flow establishment, and uncertainty

Multiple diagnostic techniques were applied in this study: coaxial thermocouples for heat transfer measurements, pressure sensitive paint for surface streak visualization, and schlieren imaging. Coaxial thermocouples are very common sensors used for the measurement of the surface temperature histories in impulse facilities. The temperature difference can be post-processed to determine the heat flux to the model. The thermocouples used in these experiments are based on the design of Sanderson.[30] They are coaxial, 2.4 mm in diameter, type E (constantan-chromel), and mount flush with the surface of the model. Due to the short test times in the HET, it can be assumed that the surface of the model is isothermal. This assumption helps simplify the analysis of the thermocouple data. This type of thermocouple gage has been used extensively in the T5 reflected shock tunnel at GALCIT,[30–32] where a response frequency of around a megahertz has been demonstrated. As a baseline case, heat transfer measurements over a flat plate in the Air-4 condition are shown in Figure 4. Data are compared with a calculation based on the model of Hayne[33] on compressible, laminar flat-plate boundary layers. Agreement between the data and prediction is generally good.

The time to establish a steady flow over the model was calculated using the method described by Gupta,[34] and the corresponding sections of the heat flux record were discarded before processing the data. Though Gupta's analysis was carried out for a flat plate in an expansion tube facility, Holden[35] reports that the same establishment times were applicable to concave ramps. Figure 5 shows a representative heat transfer trace. The extent of the horizontal lines indicates the applicable test times both with and without the correction to remove the establishment time from the ideal test time. There is a resulting difference in the average heat transfer value over the time considered. These sample data are also an indication of the degree of variation in the heat flux due to signal oscillation during the test time.

TABLE III. Vortex generator parameters.

Parameter	Value
Re_k	8755
Re_θ	504
k/δ	2

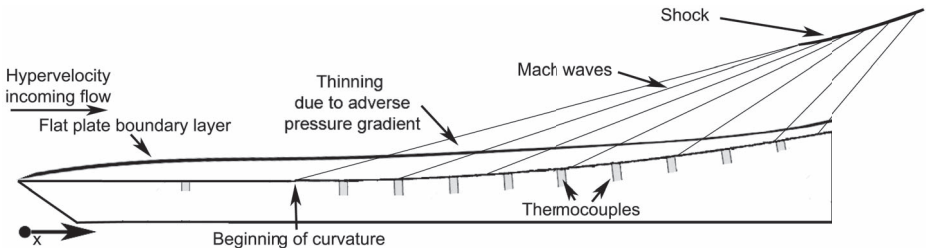

FIG. 3. Sketch of experimental setup and flow features over a concave curved surface.

Davis[31] identified two main sources of uncertainty for the thermocouple gages. First, there is error in the voltage-to-temperature conversion due to uncertainty in the NIST temperature conversion tables. Davis reports this to be 1.7% in the temperature change, which corresponds directly to a 1.7% error in the heat flux. Second, uncertainty in the thermal properties of the thermocouple materials was determined by Davis to be 8%. The uncertainties due to heat transfer fluctuations over the averaging window were taken into account by calculating a 95% confidence interval for each data point (Eq. (1)). Where ε is the absolute uncertainty, σ is the standard deviation, and n is the number of samples. The total uncertainty of each data point (combining the temperature conversion, material property, and fluctuation uncertainties) was less than 12%. More information on the implementation and validation of these gages in the HET can be found in the authors' previous work:[36]

$$\varepsilon = \frac{1.96\sigma}{\sqrt{n}}. \tag{1}$$

Pressure sensitive paints (PSPs) provide full-field data over a three-dimensional surface, a significant advantage over point gage measurements. In this study, a porous-polymer PSP was used (provided by Innovative Scientific Solutions, Inc.) which had a response time on the order of 30–50 μs.[37,38]

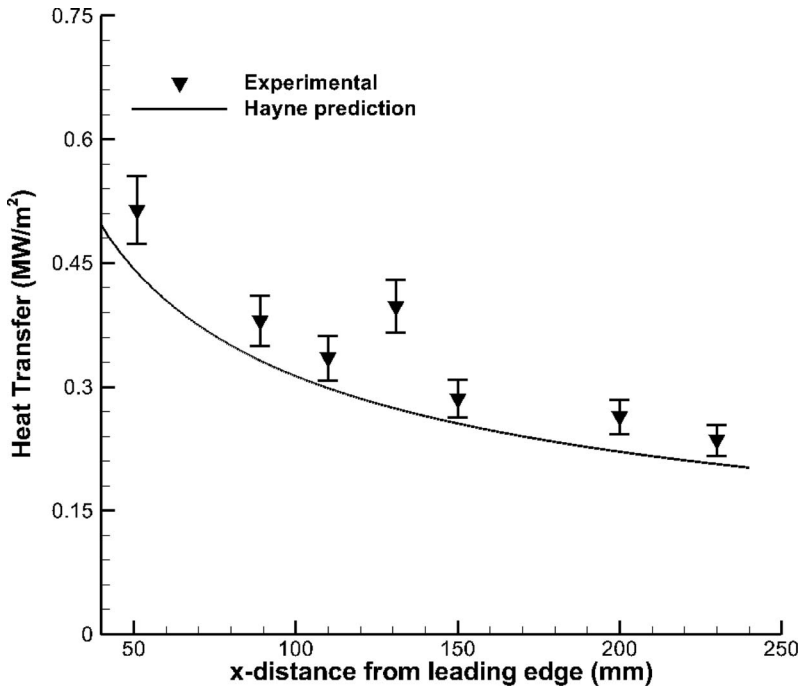

FIG. 4. Baseline measurements of heat transfer for a laminar boundary layer over a flat plate section of the full length of the models. Experimental data are compared with predictions based on the model of Hayne[33] and are in reasonable agreement.

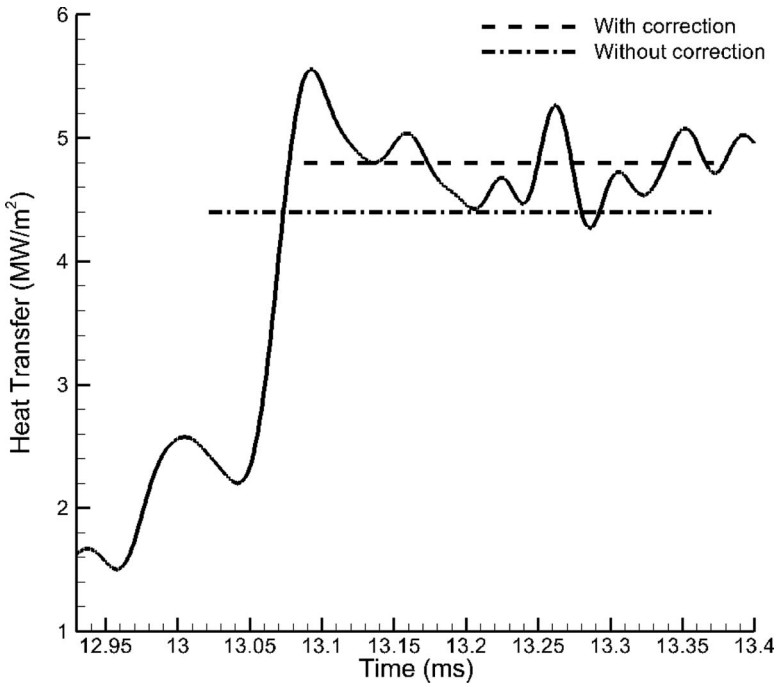

FIG. 5. A representative heat transfer trace highlighting the effect of including a correction to remove the establishment time on the calculated mean heat transfer value.

Schlieren imaging was used to visualize the boundary layer development over the models. Schlieren images show a distinct white line near the surface of the model, which previous studies have shown is due to the density gradient at the edge of the boundary layer.[39] In order to extract a quantitative visual boundary layer thickness, images were processed utilizing a MATLAB edge detection algorithm. An in-house code was then used to determine the shortest distance between the surface vector and the boundary layer vector at each downstream location. This distance necessarily lies along a vector perpendicular to the surface of the model. Schlieren images were also used to check that the location of shock formation did not interfere with the boundary layer over the curved surfaces.

III. RESULTS: LAMINAR BOUNDARY LAYERS

A. Visual boundary layer thickness measurements

The visual boundary layer thickness developing over the initial flat plate portion of the models is shown in Figure 6(a). The measured thickness is in reasonable agreement with a $\sqrt{x}$ scaling, as expected for laminar boundary layers outside the viscous interaction region. For the Curved30 model, it is possible to visualize both the initial flat plate section, as well as most of the model curvature (Figure 6(b)). The boundary layer initially grows over the flat plate portion of the model, then just after the beginning of curvature, there is an inflection point in the visual boundary layer thickness and it begins to thin.

Mohammadian[14] found that for surface geometries with the form $y \sim x^n$, for values of $n > 3/2$ the boundary layer will be supercritical (i.e., with increasing pressure, the boundary layer thickness will decrease). For supercritical conditions, the outer, supersonic layer of the boundary layer is thinning faster than the subsonic streamtube near the surface is thickening due to the pressure gradient.[40] For all the concave ramp cases presented in this work the value of n was two or greater. Thus, the observed supercritical behavior of the boundary layer is consistent with theoretical predictions.

For all curved models other than Curved30, field-of-view limitations allowed boundary layer measurements to be obtained only over the curved portions of the model (specifically from around 100 mm behind the leading edge to 180 mm behind the leading edge). Figure 7 shows the boundary

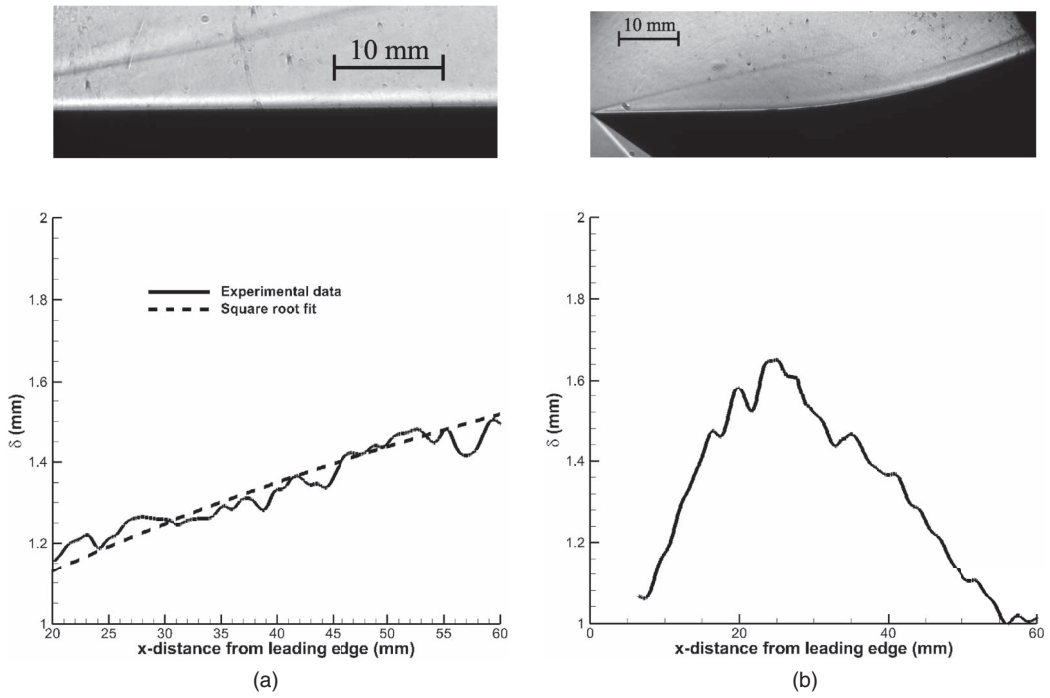

FIG. 6. Schlieren images and measured visual boundary layer thickness (δ) over (a) flat plate and (b) Curved30.

layer profiles from the four larger curved models on the same scale. The boundary layers on all four models are of similar thickness near the beginning of curvature, as expected since all begin with the same initial flat plate section. The smallest decrease in boundary layer thickness is observed over the Curved10 model, which is consistent with the fact it has the largest radius of curvature. Boundary layer profiles over Curved16 and Curved25 are similar, both in magnitude and slope, consistent with the fact that the models have very similar surface equations. There is an inflection point in the visual boundary layer thickness for Curved16 and Curved25 near 140 mm ($\theta = 9.5^\circ$). The inflection point may be an indication that the boundary layer is beginning to separate.[40] It should be noted that although the experimental data including visual boundary layer thickness and schlieren images, heat transfer and pressure measurements along the surface, show no evidence of separation along the other models, it cannot be ruled out. The Cubic32 model shows a non-constant decrease in the boundary layer thickness, which is expected since the cubic surface has a non-constant radius of

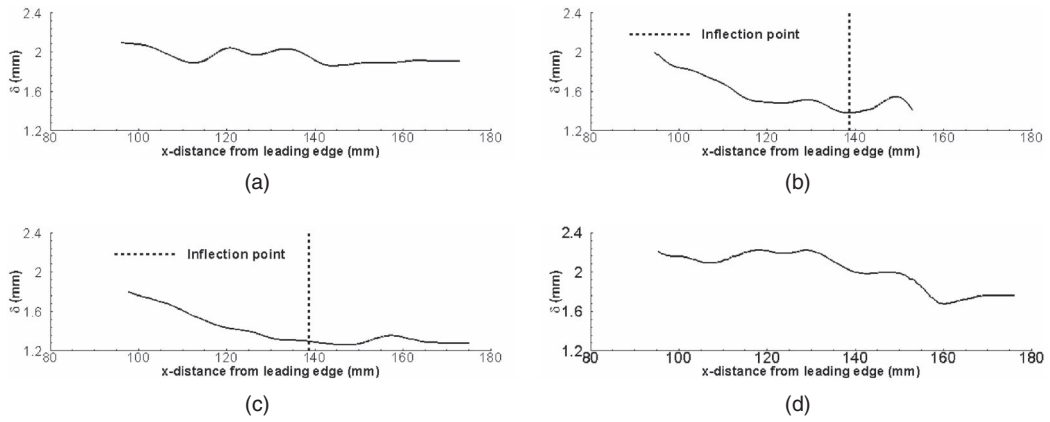

FIG. 7. Measurements of visual boundary layer thickness over the large curved models. (a) Curved10, (b) Curved16, (c) Curved25, and (d) Cubic32.

curvature. Near the beginning of curvature (where the radius would be largest) the boundary layer over Cubic32 exhibits a response similar to that over Curved10, but further downstream the boundary layer begins to thin more rapidly as the radius of curvature decreases.

B. Heat transfer measurements

Surface heat transfer measurements for the flow over each model are presented in Figures 8(a)–8(e). For the four large models, the data presented are obtained in the Air-4 test condition; for Curved30, the data presented are obtained in the Air-5 test condition. For all models considered in this study, significant augmentation in the heat transfer was measured over the sections with concave surface curvature. For the model with the smallest final turning angle, Curved10, the heat flux increased by a factor of about two, while for the other models, the heat flux increased by factors between approximately eight and 12.

Non-dimensional heat flux, $StRe^{1/2}$, where St is the Stanton number and Re is the Reynolds number, versus distance downstream for one sample data set is shown in Figure 9, together with the predictions using the approximate methods of Cohen and Reshotko,[6] Bertram and Feller,[9] and Crawford.[10] For the Stanton number calculation the heat transfer was non-dimensionalized by the freestream properties and the total enthalpy difference. The experimental data and all three predictions are in reasonable agreement for modest pressure gradients closer to the leading edge. However, at increasing distance from the leading edge, all three approximate methods severely underpredict the experimentally measured heat transfer. Significant divergence occurs by approximately 150 mm from the leading edge, which corresponds to an x/δ of 94 and a turning angle of $\theta = 11^\circ$. In this region, where the distortion to the boundary layer becomes large, the model assumptions become increasingly invalid, and the heat transfer augmentation is underpredicted by the approximate solutions by up to a factor of about five. In view of the poor agreement between experiments and approximate predictions of heat transfer augmentation at larger pressure gradients, we examine possible scalings of the experimental data over the range of surface geometries considered.

1. Heat transfer scaling with surface geometry

Curve fits were calculated for the experimental heat transfer profiles for each model geometry and are shown as solid lines in Figures 8(a)–8(e). To determine the optimal curve fit, multiple polynomial fits were generated with increasing order. Above a certain order, the R^2 value no longer improved. The optimal fit was determined by the lowest order polynomial for which there was no further increase in the R^2 value. These optimal curve fits suggested that the functional form of the heat transfer increase was of the same polynomial order as the surface equation of the model. For example, for the Curved16 model, the surface equation is a quadratic, as is the optimal fit to the heat transfer data.

To quantify this observation, scaled surface equations were calculated based on the surface equations of the models. As an example, if the model surface was described by Eq. (2), then a curve fit was determined using Eq. (3). The coefficients a and b were then selected to obtain the best fit between the scaled surface equation and the experimental data. Table IV lists the values of the a and b coefficients obtained in matching these curves for each model, together with an R^2 assessment of the fit. Each of these scaled surface fits are plotted in Figures 8(a)–8(e) as a dashed line:

$$y = c_1 x^2 + c_2 x + c_3, \tag{2}$$

$$q = a(c_1 x^2 + c_2 x + c_3) + b. \tag{3}$$

The same procedure was applied to the heat transfer data obtained for the Curved30 model, Figure 8(d), at a different test condition. The surface equations for the large models are shown in Figure 10(a), and the measured heat transfer values and the scaled surface fits are shown in Figure 10(d). Generally, good agreement is observed between the curve fits based on the surface geometry and the heat transfer data. Trends in heat transfer augmentation over the different surface geometries are captured.

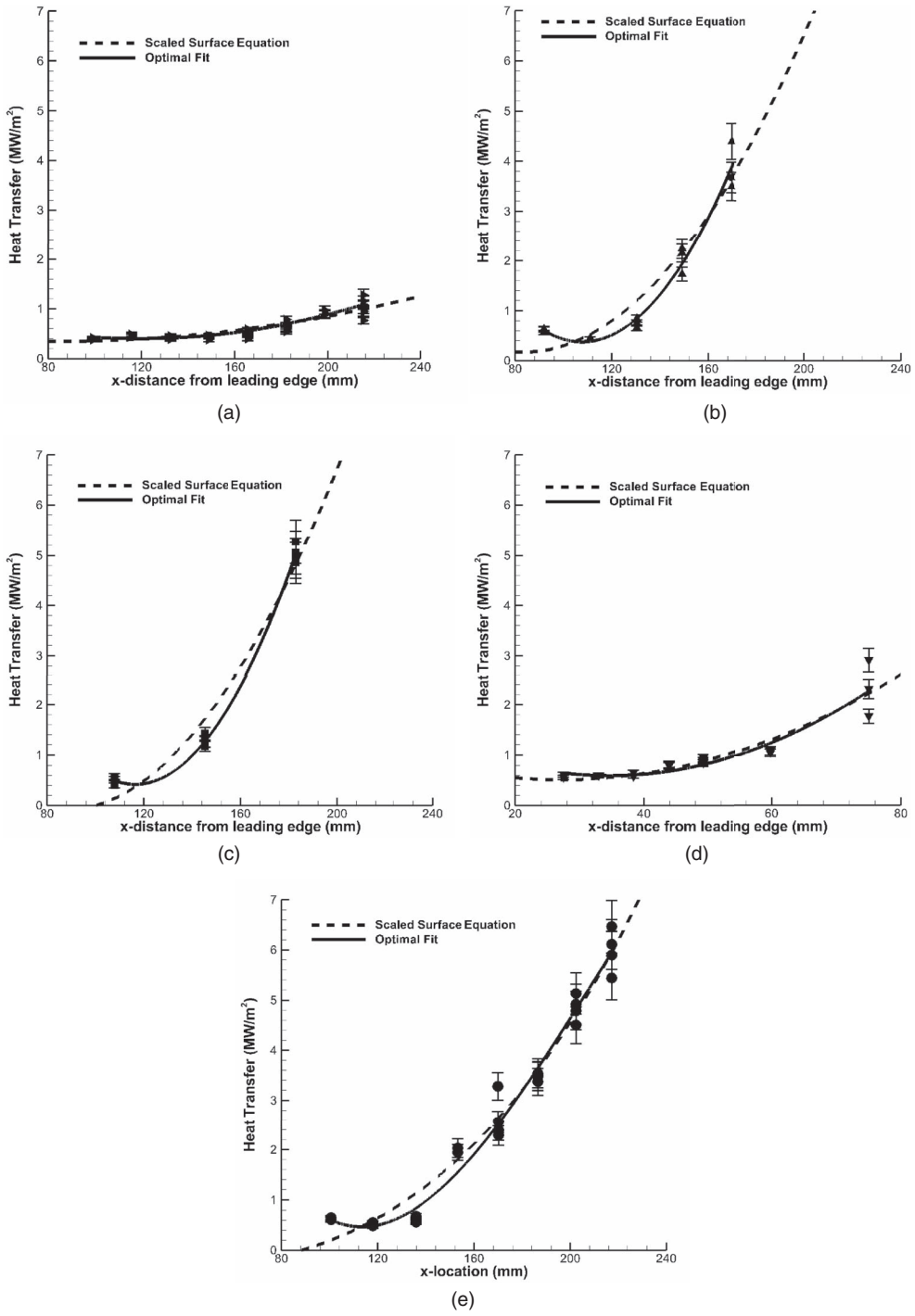

FIG. 8. Experimental heat transfer data for boundary layers developing over the different surface geometries. The solid line is a optimal curve fit to the heat transfer data, while the dashed line is the surface equation of the model with a linear scaling applied. (a) Curved10, (b) Curved16, (c) Curved25, (d) Curved30, and (e) Cubic32.

2. Heat transfer scaling with turning angle

Heat transfer data for each model are plotted versus the local turning angle (Figure 11). When turning angle, rather than distance from the leading edge, is considered, the heat transfer data for all the larger ramps collapse. The external static pressure variation with the local turning angle can

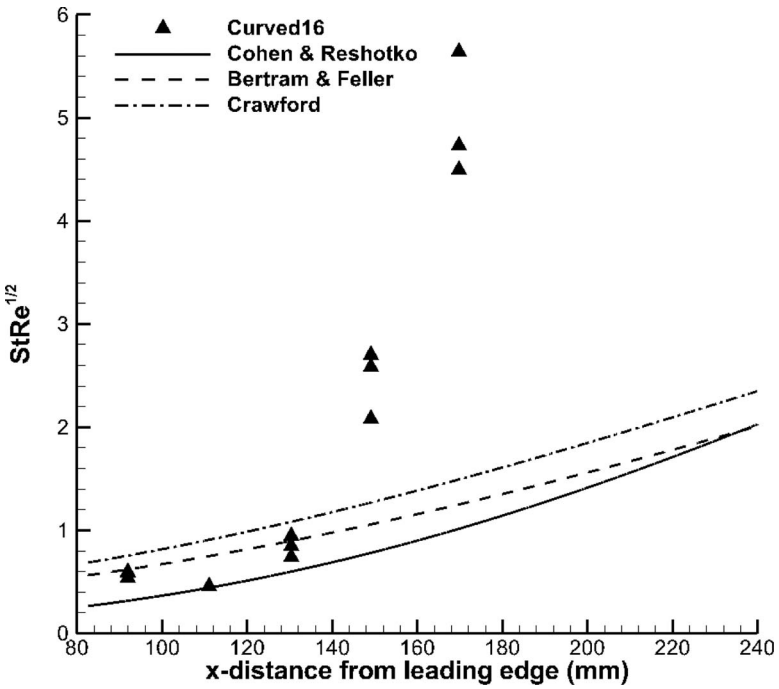

FIG. 9. Comparison of experimental heat flux data over the Curved16 model with approximate methods of Cohen and Reshotko,[4] Bertram and Feller,[9] and Crawford.[10] Agreement near the leading edge is reasonable, but the predictions diverge sharply from the experimental data around 150 mm ($\theta = 11^\circ$) downstream from the leading edge.

be calculated using the method of characteristics, and compared to the combined heat transfer data for all the models (shown as the solid line in Figure 11). The pressure profile captures the trend of the heat transfer, indicating that the effect of the curvature and pressure gradient acts locally, and the variation in the heat transfer with the turning angle is related to the isentropic compression of the flow.

In a study of laminar heat transfer over blunted bodies at hypersonic flight conditions, Lees[11] examined the magnitude of the pressure gradient term. Following Lees and assuming similarity, the momentum and energy equations become

$$\left(Cf''\right)' + ff'' + \frac{2\tilde{s}}{u_e}\frac{du_e}{d\tilde{s}}\left[\frac{\rho_e}{\rho} - \left(f'\right)^2\right] = 0, \tag{4}$$

$$\left(\frac{C}{\mathrm{Pr}}g'\right)' + fg' + \frac{u_e^2}{2h_{se}}\left[2C\left(1 - \frac{1}{\mathrm{Pr}}\right)f'f''\right]' = 0, \tag{5}$$

where $C = \rho\mu/\rho_e\mu_e$, $f' = u/u_e$, $g = h_s/h_{se}$, h_s is the total enthalpy, u is the velocity parallel to the surface, $\tilde{s}$ is the transformed coordinate about the body surface, and subscripts e and w refer

TABLE IV. Curve fit parameters used to scale the model geometry surface equations to compare with curve fits to the heat transfer data. R is the regression coefficient.

Model	a	b	R^2
Curved10	65.5	0.35	0.83
Curved16	315.9	0.16	0.92
Curved25	317.4	−0.13	0.97
Curved30	152.1	0.50	0.87
Cubic32	80.0	−0.44	0.93

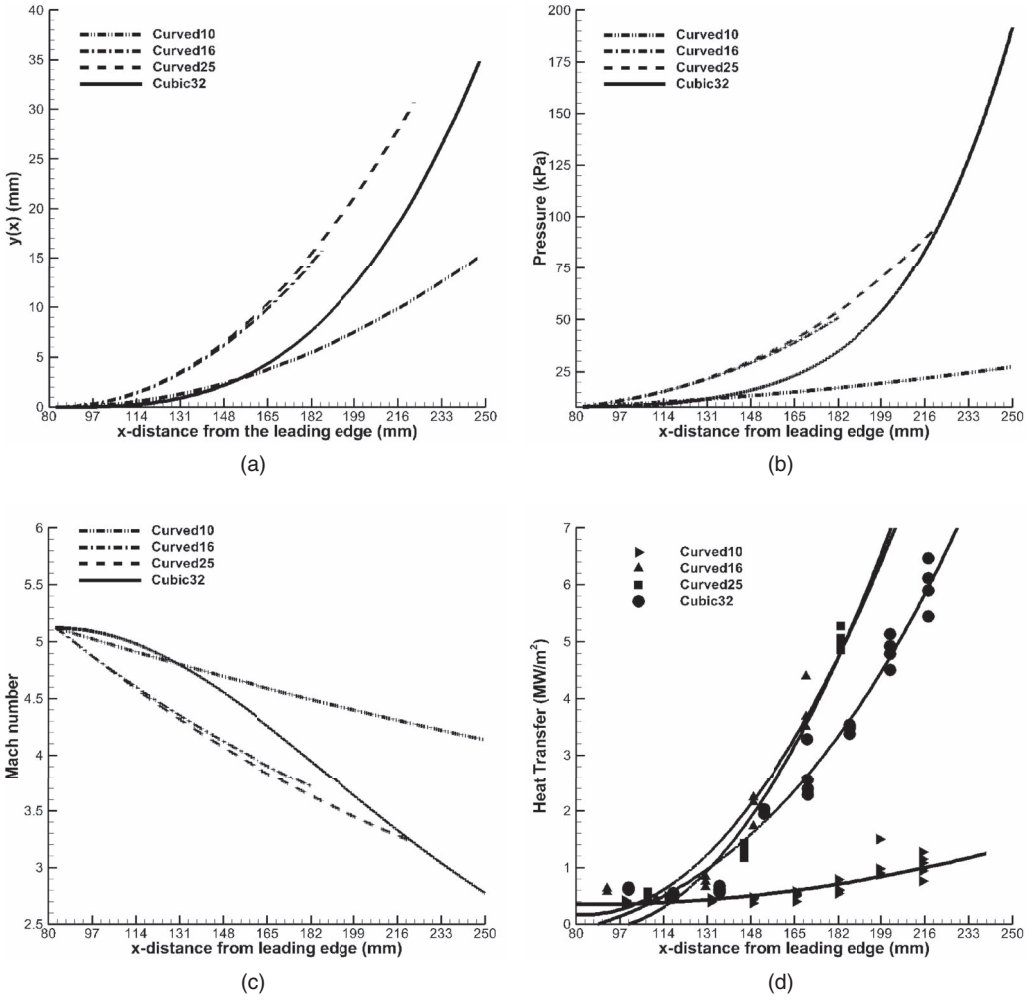

FIG. 10. (a) Model surface equations. (b) Pressure profiles for each model geometry calculated using the method of characteristics. (c) Mach number profiles for each geometry calculated with method of characteristics. (d) Experimental heat transfer measurements (symbols) and curve fits (solid lines) generated based on the model surface equations as described in the text.

to boundary layer edge and wall quantities. At hypersonic flight speeds, taking the difference in molecular weight across the boundary layer into account, Lees notes that

$$\frac{\rho_e}{\rho} \backsimeq \frac{h_s}{h_{se}} = g, \tag{6}$$

then for $g_w \ll 1$

$$g \backsimeq g_w + (1 - g_w)\frac{u}{u_e} \backsimeq \frac{u}{u_e} = f'. \tag{7}$$

The pressure gradient term in the brackets in the momentum equation thus becomes $[u/u_e - (u/u_e)^2]$, which, as evaluated by Lees, is zero at the surface and boundary layer edge and reaches a maximum value of 0.25 through the boundary layer. Thus, in the case of a highly cooled wall, where the density at the surface is much greater than at the boundary layer edge, Lees finds that to "an excellent first approximation," the influence of the pressure gradient can be neglected in comparison with the local pressure. The collapse of the heat transfer data in the present study supports this conclusion, even in the case of an adverse pressure gradient with strong boundary layer distortion, when the external pressure distribution is calculated using the method of characteristics.

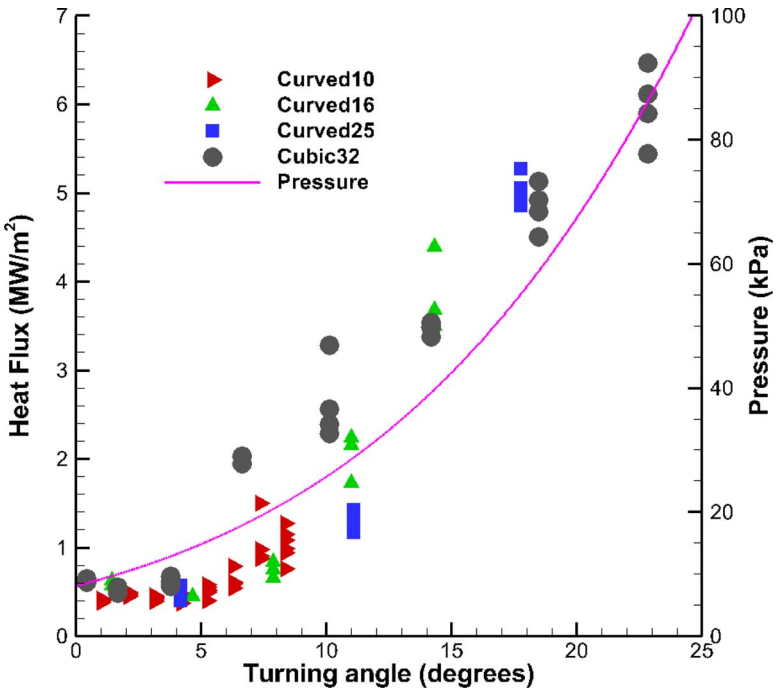

FIG. 11. Heat transfer data for laminar boundary layers over all models versus the local turning angle. The solid line is the pressure distribution calculated using the method of characteristics.

The scaling obtained in the present study was compared with available data from a previous study by Mohammadian[14] (Figure 12(a)). In that study, heat transfer was measured over a ramp with a cubic surface equation in a Mach 12.25 flow in a hypersonic gun tunnel. For clarity, in this figure, data from repeat experiments are averaged and displayed as a single point. The data of Mohammadian also appear to be in good agreement with the present experiments and data reduction strategy. For Figure 12(a), the Stanton number is calculated using the freestream conditions and stagnation enthalpy differential. Non-dimensionalization can also be performed with the boundary layer edge

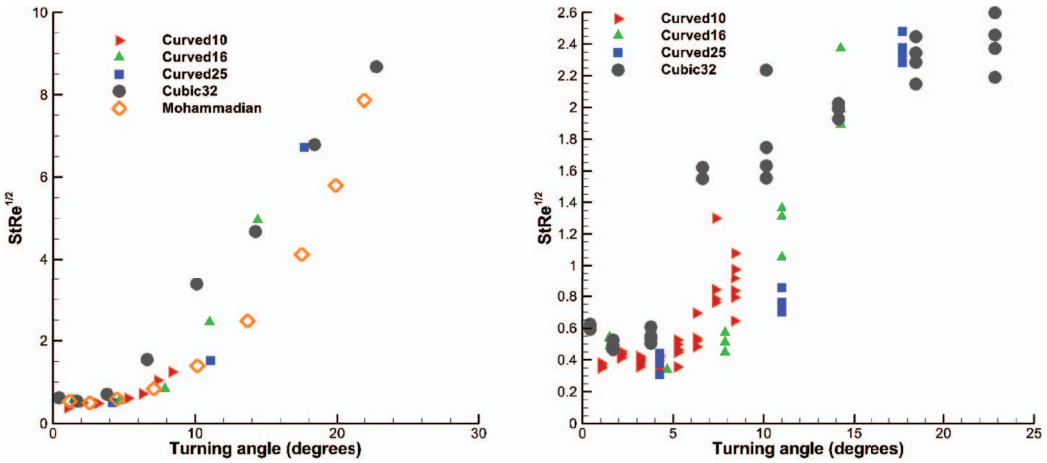

FIG. 12. (a) Comparison of nondimensional heat transfer data to results from a previous study in a different facility.[14] Good agreement is observed when all data are plotted against the local turning angle of the curved surface. Each point represents the average of repeat experiments. Non-dimensionalization calculated using freestream quantities. (b) Nondimensional heat transfer data recalculated using edge quantities rather than freestream. Reasonable estimates of heat transfer indicate freestream quantities were most likely used.

rather than the freestream quantities (Figure 12(b)). From the information in Mohammadian, it could not be determined which quantities were used, but based on reasonable estimates of heat transfer the authors believe it is correct to non-dimensionalize by the freestream values.

IV. RESULTS: BOUNDARY LAYERS WITH ADDITIONAL LOCAL DISTORTION DUE TO IMPOSED VORTEX STRUCTURES.

Boundary layers with streamwise vortices imposed by passive vortex generators are investigated both to examine the effects of additional local distortion and as a model problem for the evolution of large scale vortices subjected to adverse pressure gradients. For the baseline flat plate case, Figure 13, surface streaks are observed to form directly behind the vortex generators. Previous studies by Whitehead[24] and Berry *et al.*[29] identify similar structures in oil-flow visualization as being caused by vortices generated from similar roughness elements. Some distance downstream, the streaks are no longer clearly evident in the images. In order to determine the location at which the streaks were no longer apparent, the images were converted into binary at multiple cutoffs. Two cutoffs were then selected, the one just before the streaks were entirely saturated white, and the point just before the streaks were entirely saturated black. The streamwise extent of the streaks was

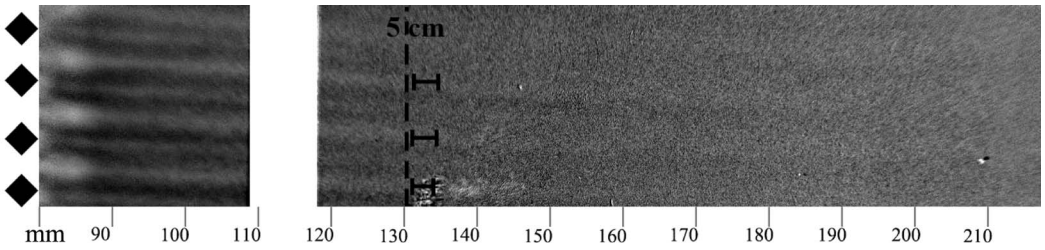

FIG. 13. Pressure sensitive paint visualization of streaks behind the vortex generators for the baseline flat plate model. The white region corresponds to location of heat transfer gages where no paint data were collected. The bottom of the image corresponds to 10 mm above the model centerline.

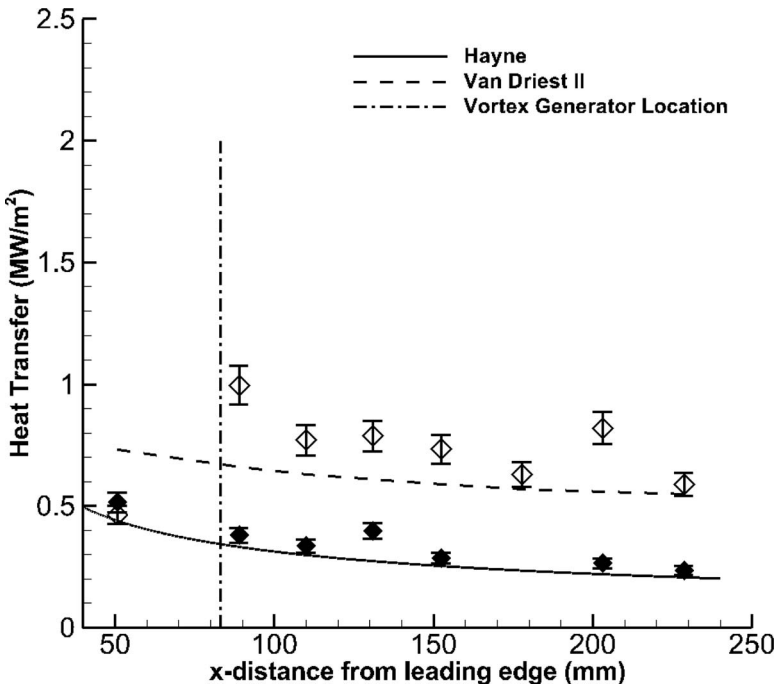

FIG. 14. Comparison of heat flux distributions over a flat plate both with (◇) and without (◆) imposed streamwise vortices. Each point represents the average of repeat experiments.

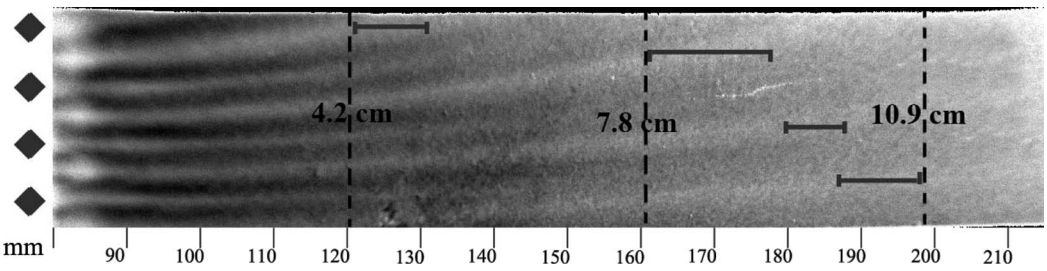

FIG. 15. Pressure sensitive paint visualization of the evolution of streaks on over a concave surface (Curved16). The bottom of the image corresponds to 10 mm above the model centerline.

determined for each image, and used to set the limits on where the structures fade from the image. For the flat plate, this range begins about 5 cm downstream of the vortex generators. It is not possible from the surface pressure paint data to determine if this is caused by the vortices breaking down or lifting off the surface.

A comparison of the heat transfer profiles for the boundary layer developing over the flat plate with and without vortex generators is presented in Figure 14. Significant heat flux augmentation is observed with the presence of the imposed structures, even at locations where the streaks are no longer visible in the PSP image. The laminar boundary layer heat flux agrees well with a prediction based on Hayne *et al.*[33] With the vortex generators installed, the heat transfer data are in better agreement with the prediction of Van Driest II for turbulent flows.[41] This should not be taken as a claim that the flow is turbulent, rather that the augmentation due to the presence of streamwise vortices is equivalent to that of a turbulent flow.

The PSP images of the Curved16 model with the vortex generators installed is shown in Figure 15. The flow features here are noticeably different from the flat plate case. The streaks are

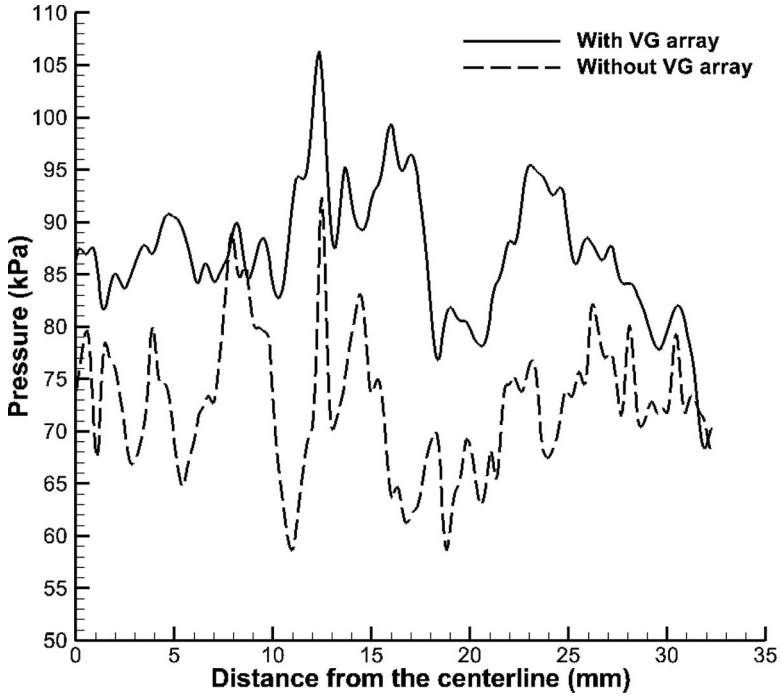

FIG. 16. Spanwise pressure distributions at 187 mm behind the leading edge extracted from PSP images of Curved16 model. Solid line is data taken with the vortex generator array installed, while the dashed line is data taken with no vortex generator array installed.

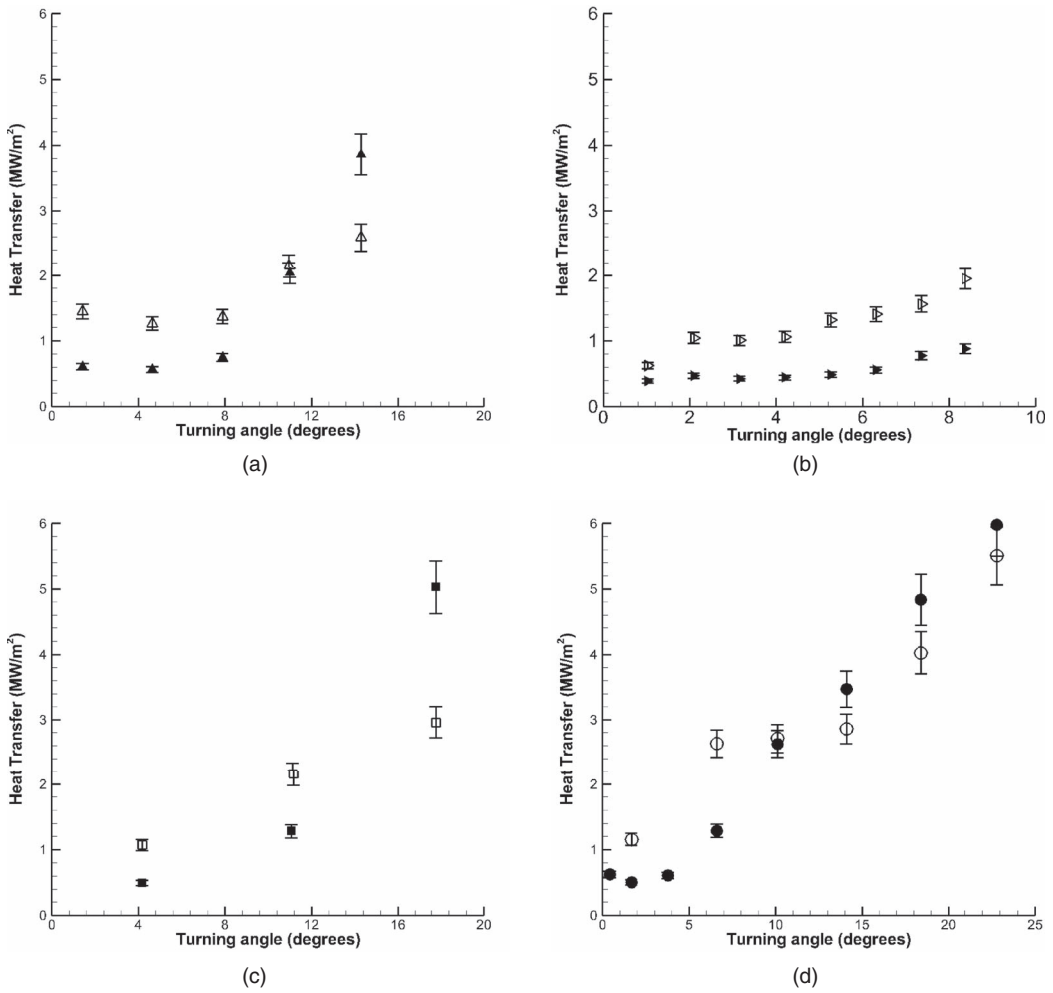

FIG. 17. Comparison of heat transfer distributions over all four large models both with (○) and without (●) imposed streamwise vorticity. Each point represents the average of repeat experiments. (a) Curved16, (b) Curved10, (c) Curved25, and (d) Cubic32.

visible on the surface for a significantly longer extent, to almost 11 cm behind the vortex generators, and the structures also appear to curve towards the edges of the model. Heat transfer data for the boundary layer developing over the Curved16 model both with and without imposed vortices are shown in Figure 17(a). For turning angles up to approximately 10° there is an augmentation to the heat transfer in the case of imposed structures. After a turning angle of 10°, however, the heat transfer relaxes to below the undisturbed values. It is possible this is caused by three-dimensional effects, and we note that a Mach cone emanating from the two corners of the leading edge would converge at approximately 153 mm downstream. Cross sections of the surface pressure data were examined and showed no detectable spanwise pressure gradient. Figure 16 shows representative spanwise pressure cross sections taken at 187 mm behind the leading edge on the Curved16 model, both with and without the vortex generator array installed. The pressure resolution of the PSP was calculated to be 0.1 kPa, thus smaller pressure gradients may be present. Additionally, the complexity of the flow could lead to interactions between the vortices, surface curvature, and adverse pressure gradient that cannot be detected with the current diagnostics, and could contribute to the reduction in heat transfer.

Similar trends are observed in the data from the Curved25 and Cubic32 models (Figures 17(c) and 17(d)). In contrast, the data for Curved10 with and without vortex generators installed show that at all measurement locations, the disturbed boundary layer exhibits increased heat transfer. For

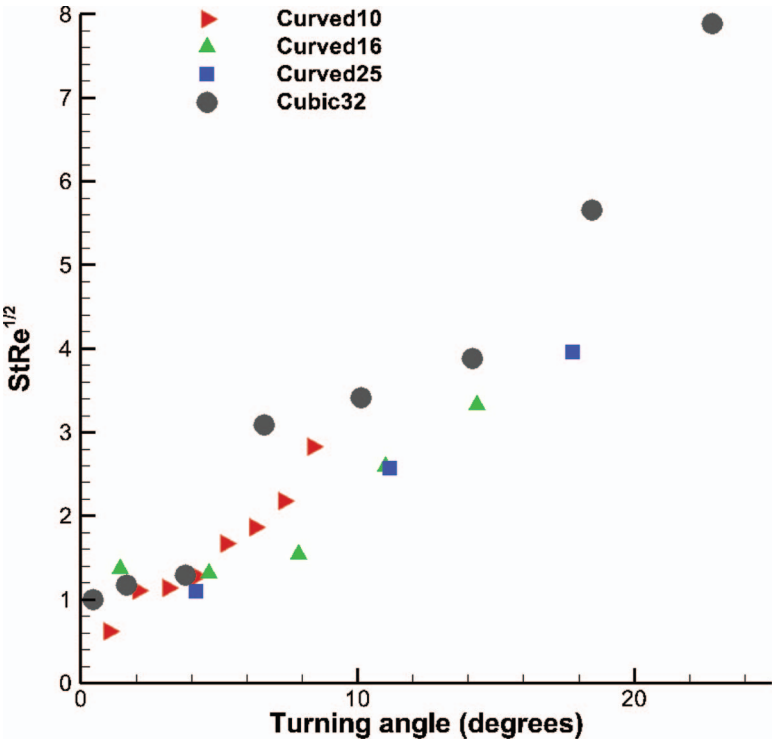

FIG. 18. Comparison of heat transfer distributions as a function of local turning angle for all surface geometries for boundary layers with imposed streamwise vortex structures. Each data point represents the average of repeat experiments.

Curved16, Curved25, and Cubic32, the transition turning angle where the disturbed boundary layer heat flux decreases to the undisturbed levels is between 10° and 12°.

A. Data reduction for models with imposed vortex structures

Heat transfer data for boundary layers with imposed vortex structures developing over the curved surfaces are shown in Figure 18 for each of the large models. Perhaps surprisingly, as for the laminar boundary layers, the data for all surface geometries collapse when the heat transfer is plotted as a function of the local turning angle of the surface. Even in the presence of additional distortions to the boundary layer, the scaling of heat flux with local turning angle identified for laminar boundary layers appears to be robust.

V. CONCLUSIONS

In this work, the response of hypervelocity boundary layers to global mechanical distortions due to concave surface curvature was investigated experimentally. Heat transfer and visual boundary layer thickness data were obtained over six model geometries with different surface equations and final turning angles. Models were designed to be interchangeable to avoid variable leading edge effects and to allow an initial laminar flat plate boundary layer to develop. Measurements of visual boundary layer thickness confirmed that, as predicted by theory, the boundary layer over each of the concave surfaces was supercritical and thinning. For the Curved16 and Curved25 models, an inflection point was observed at 140 mm downstream of the leading edge (corresponding to a turning angle of $\theta = 9.5°$ and x/δ of 97), possibly indicating the beginning of separation.

Significant augmentation in the surface heat transfer over baseline flat plate values was observed for all curvatures. Comparison of heat transfer data with approximate model predictions showed good agreement in regions of modest pressure gradient near the leading edge, but significant under-

prediction of experimental values in regions of greatest distortion. In view of this poor agreement, possible scalings of the experimental data were investigated. Curve fits to the experimental data were found to reproduce the polynomial order of the surface equations. The heat transfer data obtained for all of the large model geometries were found to collapse when plotted versus local turning angle rather than downstream distance. The collapsed data were compared with the pressure distribution calculated using the method of characteristics. Good agreement was obtained, indicating that a local scaling based on the pressure distribution and the concept of Lees' similarity can be used to predict the heat flux augmentation even in the cases of greatest distortion at the conditions of this study.

As a model problem to study the evolution of vortices, streamwise vortices were imposed into the boundary layer. The effects of the additional local distortion were investigated. Surface streaks, visualized using pressure sensitive paint, were observed to persist significantly further over a curved surface than a flat plate. For the baseline flat plate case, heat transfer augmentation due to the imposed structures was comparable to turbulent levels. For the curved surface, increases in heat transfer by factors up to 2.6 over laminar values were measured where the turning angle was less than approximately 10°. The heat transfer data for boundary layers with imposed vortex structures developing over all large models were compared. Data for all surface curvatures collapse as a function of the turning angle, as for the laminar boundary layers. Comparisons of the scaling with local turning angle and with the current heat transfer data were made with previous studies where possible, with good agreement.

ACKNOWLEDGMENTS

This work was funded through the Air Force Office of Scientific Research Young Investigator Award No. FA9550-08-1-0172 with Dr. John Schmisseur as program manager. The authors would like to thank Ryan Fontaine, Dr. Manu Sharma, Andrew Knisely, and Dr. Andy Swantek for their contributions to this work.

[1] F. M. White, *Viscous Fluid Flow*, 3rd ed. (McGraw Hill, 2006).
[2] W. S. Saric, "Gortler vortices," Annu. Rev. Fluid Mech. **26**, 379–409 (1994).
[3] A. J. Smits and J. P. Dussauge, *Turbulent Shear Layers in Supersonic Flow* (Springer, New York, 2006).
[4] C. B. Cohen and E. Reshotko, "Similar solutions for the compressible laminar boundary layer with heat transfer and pressure gradient," NACA Report No. 1293, 1956.
[5] B. Thwaites, "Approximate calculation of the laminar boundary layer," Aeronaut. Q. **1**, 245–280 (1949).
[6] C. B. Cohen and E. Reshotko, "The compressible boundary layer with heat transfer and arbitrary pressure gradient," NACA Report No. 1294, 1956.
[7] G. M. Low, "The compressible laminar boundary layer with heat transfer and small pressure gradient," NACA Report No. TN-3028, 1953.
[8] T. Li and H. T. Nagamatsu, "Hypersonic viscous flow on a noninsulated flat plate," GALCIT Report No. 25, 1955.
[9] M. H. Bertram and W. V. Fuller, "A simple method for determining heat transfer, skin friction, and boundary-layer thickness for hypersonic laminar boundary-layer flows in a pressure gradient," NASA Report No. TM 5-24-59l, 1959.
[10] D. H. Crawford, "Pressure and heat transfer on blunt curved plates with concave and convex surfaces in hypersonic flow," NASA Report No. TN D-4367, 1968.
[11] L. Lees, "Laminar heat transfer over blunt nosed bodies at hypersonic flight speeds," Jet Propul. **26**, 259 (1956).
[12] H. K. Cheng, J. G. Hall, T. C. Golian, and A. Hertzberg, "Boundary-layer displacement and leading-edge bluntness effects in high-temperature hypersonic flow," J. Aerosp. Sci. **28**(5), 353–381 (1961).
[13] J. L. Stollery, "Hypersonic viscous interaction on curved surfaces," J. Fluid Mech. **43**(3), 497–511 (1970).
[14] S. Mohammadian, "Viscous interaction over concave and convex surfaces at hypersonic speeds," J. Fluid Mech. **55**(1), 163–175 (1972).
[15] M. R. Malik and J. D. Anderson, Jr.,"Real gas effects on hypersonic boundary layer stability," Phys. Fluids A **3**(5), 803–821 (1991).
[16] G. Stuckert and H. L. Reed, "Linear disturbances in hypersonic, chemically reacting shock layers," AIAA J. **32**(7), 1384–1393 (1994).
[17] M. L. Hudson, N. Chokani, and G. V. Candler, "Linear stability of hypersonic flow in thermochemical nonequilibrium," AIAA J. **35**(6), 958–964 (1997).
[18] C. Park, *Nonequilibrium Hypersonic Aerothermodynamics* (Wiley Interscience, New York, 2000).
[19] J. H. Miller, J. C. Tannehill, G. Wadawadigi, T. A. Edwards, and S. L. Lawrence, "Computation of hypersonic flows with finite catalytic walls," J. Thermophys. Heat Transfer **9**(3), 486–493 (1995).
[20] J. F. Donovan, E. F. Spina, and A. J. Smits, "The structure of a supersonic boundary layer subject to concave wall curvature," J. Fluid Mech. **259**, 1–24 (1994).

[21] D. R. Smith and A. J. Smits, "A study of the effects of curvature and compression on the behavior of a supersonic turbulent boundary layer," Exp. Fluids **18**, 363–369 (1995).
[22] E. M. Fernando and A. J. Smits, "A supersonic turbulent boundary layer in an adverse pressure gradient," J. Fluid Mech. **211**, 285–307 (1990).
[23] I. W. Ekoto, R. D. W. Bowersox, T. Beutner, and L. Goss, "Response of supersonic turbulent boundary layers to local and global mechanical distortions," J. Fluid Mech. **630**, 225–265 (2009).
[24] A. H. Whitehead, Jr., "Flow-field and drag characteristics of several boundary-layer tripping elements in hypersonic flow," NASA Report No. TN D-5454, 1969.
[25] R. Sedney, "A survey of the effects of small protuberances on boundary-layer flows," AIAA J. **11**(6), 782–792 (1973).
[26] P. M. Danehy, A. P. Garcia, S. Borg, A. A. Dyakonov, S. A. Berry, J. A. Inman, and D. W. Alderfer, "Fluorescence visualization of hypersonic flow past triangular and rectangular boundary-layer trips," AIAA Paper No. 2007-536, 2007.
[27] C. Chang and M. M. Choudhari, "Hypersonic viscous flow over large roughness elements," AIAA Paper No. 2009-173, 2009.
[28] A. Dufrene, M. Sharma, and J. M. Austin, "Design and characterization of a hypervelocity expansion tube facility," J. Propul. Power **23**(6), 1185–1193 (2007).
[29] S. A. Berry, A. H. Auslender, A. D. Dilley, and J. F. Calleja, "Hypersonic boundary-layer trip development for Hyper-X," J. Spacecr. Rockets **38**(2), 853–864 (2001).
[30] S. R. Sanderson, "Shock wave interaction in hypervelocity flow," Ph.D. thesis (California Institute of Technology, Pasadena, CA, 1995).
[31] J. Davis, "High-enthalpy shock/boundary-layer interaction on a double wedge," Ph.D. thesis (California Institute of Technology, Pasadena, CA, 1999).
[32] A. Rasheed, "Passive hypervelocity boundary layer control using an ultrasonically absorptive surface," Ph.D. thesis (California Institute of Technology, Pasadena, CA, 2001).
[33] M. J. Hayne, D. J. Mee, S. L. Gai, and T. J. McIntyre, "Boundary layers on a flat plate at sub- and superorbital speeds," J. Thermophys. Heat Transfer **21**(4), 772–779 (2007).
[34] R. N. Gupta, "An analysis of the relaxation of laminar boundary layer on a flat plate after passage of an interface with application to expansion-tube flows," NASA Report No. TR-397, 1973.
[35] M. S. Holden, T. P. Wadhams, G. J. Smolinski, M. G. Maclean, J. Harvey, and B. J. Walker, "Experimental and numerical studies on hypersonic vehicle performance in the LENS shock and expansion tunnels," AIAA Paper No. 2006-125, 2006.
[36] W. Flaherty and J. M. Austin, "Comparative surface heat transfer measurements in hypervelocity flow," J. Thermophys. Heat Transfer **25**(1), 180–183 (2011).
[37] W. Flaherty, J. Crafton, G. Elliott, and J. M. Austin, "Application of fast pressure sensitive paint in hypervelocity flow," AIAA Paper No. 2011-848, 2011.
[38] W. Flaherty and J. M. Austin, "Experimental investigation of mechanical distortions to hypersonic boundary layers," in *28th International Symposium on Shock Waves Symposium* (The University of Manchester, Manchester, 2011), Paper No. 2431.
[39] D. R. Chapman, D. M. Kuehn, and H. K. Larson, "Investigation of separated flows in supersonic and subsonic streams with emphasis on the effect of transition," NACA Report No. TN-1356, 1957.
[40] M. S. Holden and J. R. Moselle, "Theoretical and experimental studies of the shock wave-boundary layer interaction on compression surfaces in hypersonic flow," Cornell Aeronautical Lab Report No. CAL-AF-2410-A-1, 1970.
[41] E. R. Van Driest, "Turbulent boundary layers in compressible fluids," J. Aeronaut. Sci. **18**, 145–160 (1951).